Anomalous crack arrays in anisotropic-strained manganite on scandate substrates

Changcheng Ju, Fei Xue, Fengzhen Huang, Long-Qing Chen, Xiaomei Lu, Jinsong Zhu, and Henrik Myhre Jensen

Citation: Applied Physics Letters **106**, 201905 (2015); doi: 10.1063/1.4921522
View online: http://dx.doi.org/10.1063/1.4921522
View Table of Contents: http://scitation.aip.org/content/aip/journal/apl/106/20?ver=pdfcov
Published by the AIP Publishing

Anomalous crack arrays in anisotropic-strained manganite on scandate substrates

Changcheng Ju,[1] Fei Xue,[2] Fengzhen Huang,[1,3] Long-Qing Chen,[2] Xiaomei Lu,[1,3,a)] Jinsong Zhu,[1,3] and Henrik Myhre Jensen[4]
[1]National Laboratory of Solid State Microstructures and Physics School, Nanjing University, Nanjing 210093, People's Republic of China
[2]Department of Materials Science and Engineering, The Pennsylvania State University, University Park, Pennsylvania 16802, USA
[3]Collaborative Innovation Center of Advanced Microstructures, Nanjing 210093, People's Republic of China
[4]Department of Engineering, Aarhus University, 8000 Aarhus C, Denmark

(Received 2 April 2015; accepted 10 May 2015; published online 19 May 2015)

We report that when (La,Sr)MnO_3 films grown on orthorhombic $(110)_o$ $DyScO_3$ (DSO) substrates once reach a critical thickness, anisotropic patterned cracks are introduced which propagate parallel to $[1–10]_o$ direction. The typical surface morphology and cross-sectional TEM are examined in order to clarify the formation of these cracks. The cause of crack propagation through the film and into the substrate is identified as the underlying large anisotropic strain and relatively low stiffness of DSO substrates. The electrical conduction in the crack region is found to be several orders of magnitude higher than that in the uncracked areas of the film. The energy dispersive x-ray-verified $La_{0.7}Sr_{0.3}MnO_3$ deposited into cracks may be responsible for the anomalous conducting behaviors. Finally, a simple model is constructed for estimating substrate fracture toughness and calculating an upper bound of film fracture toughness. © *2015 AIP Publishing LLC*.
[http://dx.doi.org/10.1063/1.4921522]

Over the past two decades, a multitude of new functionalities for perovskite oxides have been realized through the tuning of epitaxial strain induced by different substrates.[1–3] Strains of ~±3%, an order of magnitude higher than that presented in bulk materials, can easily be achieved in epitaxial oxide films.[4] Investigations on artificial manipulations employed in ferroelectric,[5] superconducting,[6] and multiferroic[7] transitions have yielded significant advances in this process. Rare-earth scandates with various crystal orientations,[3,5,7] such as $DyScO_3$, $GdScO_3$, and $TbScO_3$, have proven to be excellent substrate candidates aiming for productions of large tensile strains. In the case of strained mixed-valance manganite, Wang *et al.* recently presented that ultra-thin $La_{0.7}Sr_{0.3}MnO_3$ (LSMO) film on (110)-orientated $DyScO_3$ substrate reveals abnormal in-plane transport anisotropy because of the underlying tensile strain.[8] In addition, it has also been discovered that the preference of phase separation in manganite could be controlled.[9]

However, when films are thicker, defects occur occasionally even leading to cracks. These structural defects would probably involve great changes in the functionality of thin films.[10] For example, both Ovsyannikov *et al.*[11] and Biegalski *et al.*[12] reported that visible cracking on the surface of films deposited on $DyScO_3$ (DSO) substrates would cause irreproducible transport or dielectric performances. In some cases, cracks have propagated through the entire thickness of a film.[13] Here, we investigate the features of cracks produced in $(001)_{pc}$ LSMO films on $(110)_o$-orientated $DyScO_3$ substrate above the critical thickness[12] with the aim of elucidating the configuration of cracks in rare-earth scandate substrates (the pseudo-cubic and orthorhombic index denoted by the 'pc' and 'o' subscripts, respectively). Crack arrays are induced by large anisotropic strain and propagation originates in the film. Then, by the difference in stiffness between film and substrate, cracks further move into the substrate.

Using standard pulsed laser deposition methods, high-quality epitaxial 100 nm LSMO film was deposited on commercially available $(110)_o$ DSO substrates and $(001)_c$ $SrTiO_3$ (STO) for comparison (substrates all obtained from CrysTec GmbH, and the subscript "c" represents cubic structures). The LSMO thin film was grown with a KrF excimer laser operated at 10 Hz with a laser energy density of 1.5 J/cm^2. The optimal oxygen atmosphere was 100 mTorr, and the growth temperature was 700 °C for the STO substrate and 20 °C higher for DSO. While STO is a cubic perovskite with a = b = 3.905 Å, DSO has orthorhombic structure, and the lattice parameters of its $(110)_o$ surface are a = 3.951 Å along the $[001]_o$ direction and b = 3.946 Å along the $[1–10]_o$ direction.[8] Figure 1 shows the orientation relationships of thin films to the substrates. The calculated biaxial strain, $\varepsilon_{sx} = (a_{subx} - a_{filmx})/a_{filmx}$ (x = a or b), is also identified in Fig. 1(a), where a_{film} is the lattice parameter of bulk LSMO, 3.873 Å, and a_{sub} is the in-plane lattice parameter of substrates.[13] In spite of the ~1.9% overall tensile strain, large in-plane anisotropy of ~0.13% is verified for LSMO on DSO. Figure 1(b) provides the lattice anisotropy of the orthorhombic structures along with the elastic modulus of both LSMO and the scandates themselves, which may help us to further understand the inevitability of defect formations.[14–16]

Figures 2(a) and 2(b) are images of the typical surface morphology of 15 nm and 100 nm-thick LSMO film on DSO

a)Electronic mail: xiaomeil@nju.edu.cn

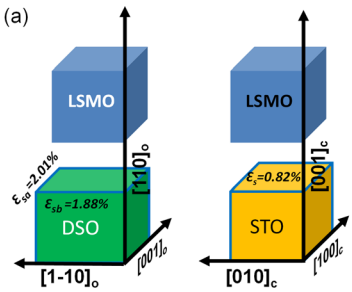

(b)

Materials	Lattice parameters (Å)	Calculated Young's Modulus (Gpa)
LSMO[13] (p-cubic)	$a[100]_{pc}$= $b[010]_{pc}$= 3.873	$Y[100]_{pc}$= $Y[010]_{pc}$= 430
STO[5, 13] (cubic)	$a[001]_c$= $b[010]_c$= 3.905	$Y[001]_c$= $Y[010]_c$= 361
DSO[14,15] (ortho)	$a[001]_o$= 3.951, $b[1\text{-}10]_o$=3.946	$Y[001]_o$= 184, $Y[1\text{-}10]_o$=222

FIG. 1. (a) Crystal structures of pseudocubic LSMO and substrates of STO and DSO. Lattice mismatches between the films and underlying substrates are also indicated. (b) Comparison of the elastic tensors and lattice parameters of the rare-earth scandate DSO, the cubic substrate STO, and the pseudo-cubic LSMO along certain orientations.

obtained by atomic force microscopy (AFM) (Veeco MultiMode 8). The surface morphology of the 15 nm LSMO film on DSO is atomically flat with terraces separated by steps about 4 Å high, which suggests layer by layer growth of the film. This is in accordance with previous work with fully strained ultrathin LSMO films,[8] in which unit cell level steps could be observed on films under both compressive and tensile strains. As to 100 nm LSMO film, we observe similar steps on LMSO/STO surface (published elsewhere). However, when imaging a 16 × 16 μm^2 region of 100 nm LSMO/DSO thin film, evidences of strain relaxation can be seen in the formation of linear surface protrusions that propagate along $[1-10]_o$ direction shown in Fig. 2(b). Importantly, layer by layer growth features appear between the protrusions as well, revealing a refined growth mode of the whole film. The average height of the protruding lines is 1.5 nm above the smooth surface, and they occur at intervals of 1.0–7.2 μm. These features are commonly seen in strained semiconductor materials and have been observed in films under both tensile and compressive stresses.[17,18] Analogous surface features also appear in $SrTiO_3$ and $SrFeO_3$ films under biaxial tensile strain.[12,19] Furthermore, given that three-dimensional islands[3] are mostly observed with isotropic in-plane strain, these cracks, only in single direction, call attention to the anisotropy of the elastic stress.[10,12] On examination under higher resolution in Fig. 2(c), it can be seen that the lines protruding above the surface are associated with the cracks inside. As shown in Fig. 2(d), within the accuracy of AFM tips, the crack center is revealed to be about 2 nm lower than the edges, spanning a width of 28 nm. When the film reaches a thickness larger than 150 nm, the cracks propagate along two axes in the inset of Fig. 3. That means 150 nm thin film is above critical thickness of cracking along both axes, whereas 100 nm is above critical thickness along the $[1-10]_o$ axis and below that along the $[001]_o$ axis.

To investigate the conduction properties of both the cracks and films, local electrical conductivity was measured using high-resolution conductive atomic force microscopy (c-AFM) by applying biased voltage between the Pt-Ir-coated AFM tip and the silver colloid contact on one side of the sample.[20] Using this method, irreproducible macroscopic transport performance was avoided.[11] Usually, LSMO film (on $LaAlO_3$ or DSO) acts as an insulator under large compressive or tensile strains,[8,21] but exhibits metallic behavior under small strains.[22] With a measuring tip bias of positive

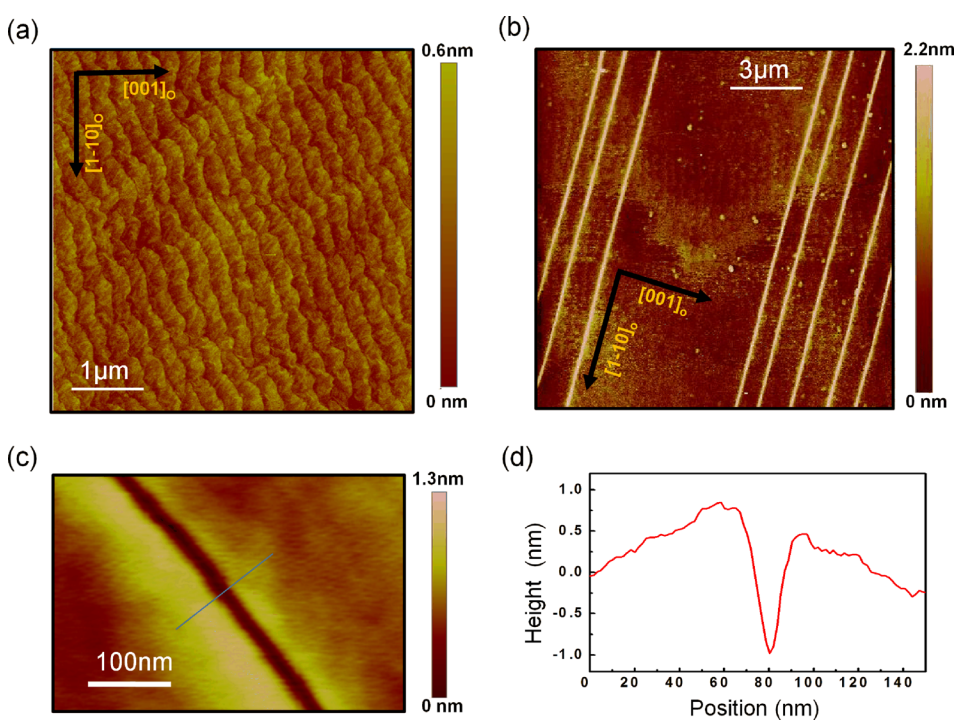

FIG. 2. AFM images of (a) 15 nm LSMO/DSO with unit-cell-high steps on the surface; (b) 100 nm LSMO/DSO thick films showing surface cracks and a very flat surface. (c) High-resolution AFM image of cracks featured in Fig. 2(b). (d) Line scan along the $[001]_o$ in-plane direction of the DSO substrate showing the height of the crack region. The blue line in Fig. 2(c) represents the scanning path.

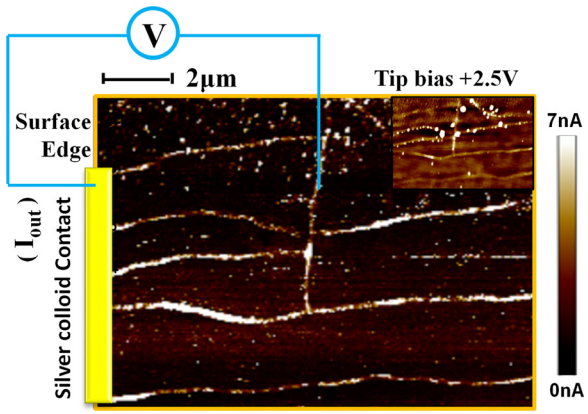

FIG. 3. C-AFM image of more than 150 nm-thick LSMO/DSO sample showing conduction of the crack arrays. The inset figure is the corresponding morphology image taken within C-AFM measurements.

2.5 V, electrical conduction currents at the crack lines reached as high as 6.8 nA, as shown in Fig. 3. In contrast, the current signals of film regions without cracks are barely detectable within the voltage limit, meaning that the resistivity of these regions is several orders larger than that of the crack lines. In previous works, anisotropic conductions in strained magnets were mostly related to the preference of metallic domain orientations,[9] hybridization between O $2p_x$ and Mn $3d$ orbitals,[8] and unbalanced orbital populations.[23] However, in our case, the percolative conduction of filamentous crack arrays is preferential in [1−10] direction with smaller strains, which could be another possible origin for the globe anisotropic transport behaviors.

Figure 4(a) is a cross-sectional TEM image of LSMO/DSO with three typical crack arrays. Unlike some previous reports,[5,12] the cracks are not limited to the LSMO layer but penetrate the interface and propagate into the substrate instead. The distance between neighboring cracks is about 1 μm, which is consistent with the surface morphology shown in Fig. 2(b). Figure 4(b) is a HAADF-STEM image of the cracking area, enlarged,[24] with the interface between LSMO and the DSO substrate demarcated by a dashed line. Aside from the cracking area, the interface is perfectly coherent, indicating that the film has a uniform LSMO structure except in the cracking region. It must also be noted that with the 100 nm thick film, cracks propagate as deep as 300 nm into the substrate.

Fig. 4(c), the magnified red dashed box within Fig. 4(b), is the high-resolution TEM image of the bottom of the crack within the DSO substrate. According to the color contrast in the bright field shown in the figure, the cracks are filled with uniform materials. The as-grown materials inside the crack are tightly surrounded by a single crystalline DSO phase and evidence that the cracks form during the deposition process and not the cooling period. Aside from dislocations, crack formation is the primary mechanism through which films relieve the elastic strain. To determine the materials in cracks within the thin film, energy dispersive x-ray (EDX) line scans were performed in the LSMO layer across the crack on the cross-sectional sample, as indicated by the blue arrow in Fig. 4(b). Figure 4(d) shows the corrected La, Sr, Mn, and O

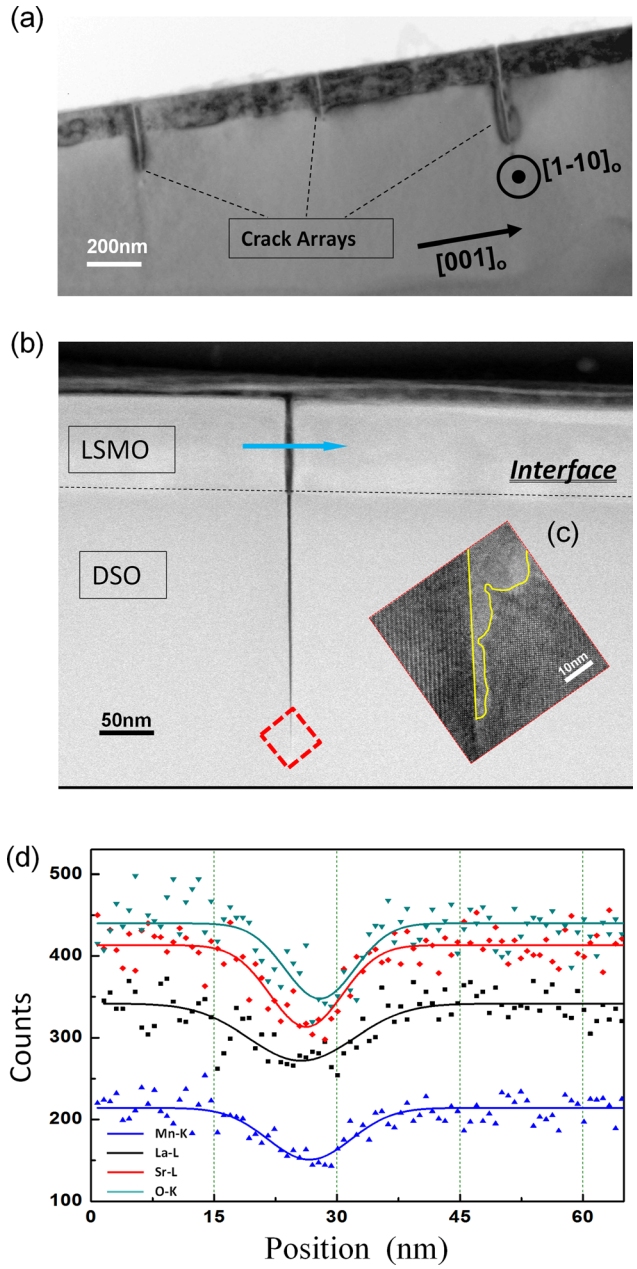

FIG. 4. (a) A typical cross-sectional TEM of the cracked area taken along $[1-10]_o$ zone axis, with periodic crack penetration in the DSO substrate. (b) A HAADF-STEM of a single crack. (c) A high magnification cross-sectional TEM showing the crack termination in the DSO substrate. (d) EDX analysis showing the elemental composition across a single crack in LSMO.

signals and that the stoichiometry of uncracked region is the same as that of the nominal composition. In the cracked region, the intensity ratio of La(Sr)/Mn/O is subtly altered and lower than that of the uncracked region, but no obvious diffusion signals of Dy, Sc elements[25] are detected. The relatively lower intensity indicates poor crystalline quality probably due to low thermal conduction inside the cracks. Therefore, the verified LSMO with stress-free boundary conditions[21] is more metallic than the uncracked region and may be responsible for the anomalous conducting behaviors found in the insulating film. Recently, Du *et al.*[26] reported that ferromagnetic-metallic phase could be induced by edge states in μm-wide $La_{0.325}Pr_{0.3}Ca_{0.375}MnO_3$ strips, which

have strong influence on the transport properties. In our samples, the numerous as-grown crack edge states may also contribute to the enhanced conductance.

On the basis of the experimental results, we now focus on the origin of the conductive crack arrays. As previously mentioned, the cracks are observed to propagate through the film and into the substrate as expected in cases where film stiffness is higher than substrate stiffness.[27] The sketch provided in Fig. 5 represents a simple model for estimating the fracture toughness of DSO substrate with 100 nm LSMO thin film. Using the residual stress σ, and the film thickness t, its membrane force, or P, can be estimated as $P = \sigma \cdot t$. Considering that the film and substrate are linear elastic, the membrane force can be further simplified as $P = Y_{\mathrm{LSMO}} \cdot \varepsilon_s \cdot t = 800\,\mathrm{N/m}$. According to standard fracture mechanical solutions,[28] the mode I stress intensity factor, K_{I}, can then be estimated as

$$K_I = \frac{2P}{\sqrt{\pi d}} \frac{1.3 - 0.3\left(t/(2d)\right)^{5/4}}{\sqrt{1 - \left(t/(2d)\right)^2}}, \tag{1}$$

where d ($d > t$) denotes crack depth. This expression for stress intensity factor neglects the effects of elastic mismatch between the film and substrate. However, extensive numerical analyses of the errors involved in this assumption[29–31] have shown that (1) is sufficient for the present purpose. For the film/substrate arrangement investigated in this work, (1) yields a critical substrate fracture toughness of $K_{\mathrm{Ic}} = 1.6\ \mathrm{MN/m^{3/2}}$, resulting in a fracture energy of $G_c = K_{\mathrm{Ic}}^2 / Y_{\mathrm{LSMO}} = 12\,\mathrm{J/m^2}$. Additionally, assuming that an edge crack has propagated through the film up to the interface (meaning that crack length is equal to film thickness), an upper bound for film fracture toughness can also be estimated. The stress intensity factor for an edge crack with the crack depth $d = t$ can be calculated as[28]

$$K_I = 1.12\sigma\sqrt{\pi t}, \tag{2}$$

resulting in a critical film fracture toughness of $K'_{\mathrm{Ic}} = 5\ \mathrm{MN/m^{3/2}}$. If the fracture toughness is less than this value ($K_{\mathrm{Ic}} < K'_{\mathrm{Ic}}$), cracks are expected to exceed the LSMO film. From Eq. (1), we can generally deduce that the risk of cracks propagating into the substrate is reduced if film thickness is reduced because the membrane force, main factor affecting the stress intensity factor, is also reduced. Therefore, the competition of critical fracture toughness between thin film and substrates is crucial to the crack configurations, and the application of DSO substrates for large tensile strain should pay close attention to the limitations caused by film thickness.

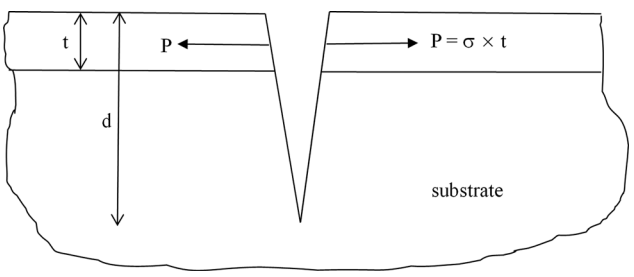

FIG. 5. Schematics of the geometry for estimating fracture toughness.

In conclusion, we fabricated tensile strained perovskite LSMO on DSO substrate and examined the formation of $[1-10]_o$-parallel crack arrays in the thin film, indicating the anisotropic strain relaxation process. The presence of cracks that propagated through the film into the substrate reveals the significant influence of substrate stiffness on cracking, a factor that is often neglected in typical analyses of epitaxial growth. As most rare-earth scandates have a structure similar to DSO,[14] future investigations utilizing large strains should pay careful attention to the stiffness difference of film/substrate system and thickness limitation in order to avoid cracking. In the meantime, engineering of the conducting as-grown LSMO channels in insulating regime may expand our understanding of domain wall type nanoelectronics and help to develop functional devices.

This work was supported by National Natural Science Foundation of China (Nos. 51225201 and 61271078), the 973 Project of MOST (No. 2015CB921201), the Priority Academic Program Development of Jiangsu Higher Education Institutions (PAPD) and Fundamental Research Funds for the Central Universities.

[1]J. Cao and J. Wu, Mater. Sci. Eng. R **71**, 35 (2011).
[2]A. J. Millis, Nature (London) **392**, 147 (1998).
[3]L. W. Martin, Y.-H. Chu, and R. Ramesh, Mater. Sci. Eng. R **68**, 89 (2010).
[4]D. G. Schlom, L.-Q. Chen, C.-B. Eom, K. M. Rabe, S. K. Streiffer, and J.-M. Triscone, Annu. Rev. Mater. Res. **37**, 589 (2007).
[5]J. H. Haeni, P. Irvin, W. Chang, R. Uecker, P. Reiche, Y. L. Li, S. Choudhury, W. Tian, M. E. Hawley, B. Craigo, A. K. Tagantsev, X. Q. Pan, S. K. Streiffer, L. Q. Chen, S. W. Kirchoefer, J. Levy, and D. G. Schlom, Nature (London) **430**, 758 (2004).
[6]I. Bozovic, G. Logvenov, I. Belca, B. Narimbetov, and I. Sveklo, Phys. Rev. Lett. **89**, 107001 (2002).
[7]J. H. Lee, L. Fang, E. Vlahos, X. Ke, Y. W. Jung, L. F. Kourkoutis, J.-W. Kim, P. J. Ryan, T. Heeg, M. Roeckerath, V. Goian, M. Bernhagen, R. Uecker, P. C. Hammel, K. M. Rabe, S. Kamba, J. Schubert, J. W. Freeland, D. A. Muller, C. J. Fennie, P. Schiffer, V. Gopalan, E. Johnston-Halperin, and D. G. Schlom, Nature (London) **466**, 954 (2010).
[8]B. M. Wang, L. You, P. Ren, X. M. Yin, Y. Peng, B. Xia, L. Wang, X. J. Yu, S. M. Poh, P. Yang, G. L. Yuan, L. Chen, A. Rusydi, and J. L. Wang, Nature Commun. **4**, 2778 (2013).
[9]T. Z. Ward, J. D. Budai, Z. Gai, J. Z. Tischler, L. F. Yin, and J. Shen, Nat. Phys. **5**, 885 (2009).
[10]T. Zhu and J. Li, Prog. Mater. Sci. **55**, 710 (2010).
[11]G. A. Ovsyannikov, A. M. Petrzhik, I. V. Borisenko, A. A. Klimov, Yu. A. Ignatov, V. V. Demidov, and S. A. Nikitov, J. Exp. Theor. Phys. **108**, 48 (2009).
[12]M. D. Biegalski, D. D. Fong, J. A. Eastman, P. H. Fuoss, S. K. Streiffer, T. Heeg, J. Schubert, W. Tian, C. T. Nelson, X. Q. Pan, M. E. Hawley, M. Bernhagen, P. Reiche, R. Uecker, S. Trolier-McKinstry, and D. G. Schlom, J. Appl. Phys. **104**, 114109 (2008).
[13]L. M. Berndt, V. Balbarin, and Y. Suzuki, Appl. Phys. Lett. **77**, 2903 (2000).
[14]M. Janovská, P. Sedlák, H. Seiner, M. Landa, P. Marton, P. Ondrejkovič, and J. Hlinka, J. Phys.: Condens. Matter **24**, 385404 (2012).
[15]P. Sedlák, H. Seiner, J. Zídek, M. Janovská, and M. Landa, Exp. Mech. **54**, 1073 (2014).
[16]R. O. Bell and G. Rupprecht, Phys. Rev. **129**, 90 (1963).
[17]A. Vailionis, B. Cho, G. Glass, P. Desjardins, D. G. Cahill, and J. E. Greene, Phys. Rev. Lett. **85**, 3672 (2000).
[18]K. H. Nam, I. H. Park, and S. H. Ko, Nature **485**(7397), 221–224 (2012).
[19]H. Yamada, M. Kawasaki, and Y. Tokura, Appl. Phys. Lett. **80**, 622 (2002).
[20]J. Seidel, L. W. Marttin, Q. He, Q. Zhan, Y. H. Chu, A. Rother, M. E. Hawkridge, P. Maksymovych, P. Yu, M. Gajek, N. Balke, S. V. Kalinin,

S. Gemming, F. Wang, G. Catalan, J. F. Scott, N. A. Spaldin, J. Orenstien, and R. Ramesh, Nat. Mater. **8**, 229 (2009).
[21]F. Yang, N. Kemik, M. D. Biegalski, H. M. Christen, E. Arenholz, and Y. Takamura, Appl. Phys. Lett. **97**, 092503 (2010).
[22]Y. Takamura, R. V. Chopdekar, E. Arenholz, and Y. Suzuki, Appl. Phys. Lett. **92**, 162504 (2008).
[23]S. Dong, S. Yunoki, X. Zhang, C. Sen, J.-M. Liu, and E. Dagotto, Phys. Rev. B **82**, 035118 (2010).
[24]B. Wiedenhorst, C. Höfener, Y. Lu, J. Klein, L. Alff, B. H. Freitag, and W. Mader, Appl. Phys. Lett. **74**, 3636 (1999).
[25]Y. J. Li, J. Wang, Y. S. Yin, and H. J. Ma, Bull. Mater. Sci. **28**, 69 (2005).
[26]K. Du, K. Zhang, S. Dong, W. G. Wei, J. Shao, J. B. Niu, J. J. Chen, Y. Y. Zhu, H. X. Lin, X. L. Yin, S.-H. Liou, L. F. Yin, and J. Shen, Nat. Commun. **6**, 6179 (2015).
[27]J. L. Beuth, Int. J. Solids Struct. **29**, 1657 (1992).
[28]H. Tada, P. Paris, and G. C. Irwin, *The Stress Analysis of Cracks Handbook* (Paris Productions, 1985).
[29]S. Steffensen, N. D. Madsen, and H. M. Jensen, Int. J. Solids Struct. **50**, 3406 (2013).
[30]S. Steffensen and H. M. Jensen, Eur. J. Mech. **43**, 133 (2014).
[31]S. Steffensen and H. M. Jensen, Comput. Mater. Sci. **98**, 263 (2015).